Science Advances
AAAS

Supplementary Materials for

A multifunctional electronic skin based on patterned metal films for tactile sensing with a broad linear response range

Min Cai, Zhongdong Jiao, Shuang Nie, Chengjun Wang, Jun Zou, Jizhou Song*

*Corresponding author. Email: jzsong@zju.edu.cn

Published 22 December 2021, *Sci. Adv.* **7**, eabl8313 (2021)
DOI: 10.1126/sciadv.abl8313

This PDF file includes:

Supplementary Notes

Note S1: Decoupling of pressure and temperature sensing.

The multiple stimuli of temperature and pressure on the sensing pixel will induce the relative resistance changes in P/T-unit as

$$\frac{\Delta R_{P-unit}}{R^0_{P-unit}} = K^P_{P-unit} \cdot \Delta P + K^T_{P-unit} \cdot \Delta T \,,\ \frac{\Delta R_{T-unit}}{R^0_{T-unit}} = K^P_{T-unit} \cdot \Delta P + K^T_{T-unit} \cdot \Delta T \,. \quad (1)$$

Here, R^0_{P-unit} and R^0_{T-unit} are the initial resistance of P-unit and T-unit, respectively; ΔR_{P-unit} and ΔR_{T-unit} are the resistance change of P-unit and T-unit, respectively; ΔP and ΔT represent the change of pressure and temperature, respectively; K^P_{P-unit} and K^P_{T-unit} are the pressure sensitivity of P-unit and T-unit, respectively; K^T_{P-unit} and K^T_{T-unit} are the temperature sensitivity of P-unit and T-unit, respectively. The same structure and material designs of patterned metal films for P-unit and T-unit yield the same temperature sensitivity, i.e., $K^T_{P-unit} = K^T_{T-unit}$. The microprotrusion design on the P-unit enhances the pressure sensitivity of P-unit significantly while the pressure sensitity of T-unit remains negligible such that Equation (1) can become

$$\frac{\Delta R_{P-unit}}{R^0_{P-unit}} = K^P_{P-unit} \cdot \Delta P + K^T_{T-unit} \cdot \Delta T \,,\ \frac{\Delta R_{T-unit}}{R^0_{T-unit}} \approx K^T_{T-unit} \cdot \Delta T \,. \quad (2)$$

The temperature and pressure changes can then be obtained as

$$\Delta T = \frac{1}{K^T_{T-unit}} \cdot \frac{\Delta R_{T-unit}}{R^0_{T-unit}} \,,\ \Delta P = \frac{1}{K^P_{P-unit}} \cdot \left(\frac{\Delta R_{P-unit}}{R^0_{P-unit}} - \frac{\Delta R_{T-unit}}{R^0_{T-unit}}\right) . \quad (3)$$

All variables on the right-hand side of Eq. (3) are measurable or can be calibrated.

Note S2: Pressure analysis of the sensing pixel.

Three-dimensional (3D) finite element models were established in ABAQUS to investigate the strain distributions of the P-unit and the T-unit subjected to a pressure, respectively. The P-

unit consisted of a layer of serpentine metal (chromium/gold) trace sandwiched by the patterned PI layers with a spatially distributed SU-8 micro-protrusion array on the P-unit, while the T-unit only consisted of a layer of serpentine metal (chromium/gold) trace sandwiched by the patterned PI layers, as illustrated in Fig. 1d and 1e. The P/T-unit were bonded onto a soft PDMS substrate. The thicknesses of PDMS, chromium, gold and PI were 100 μm, 5 nm, 60 nm, and 5 μm, respectively. The chromium layer was neglected in the finite element model due to its extremely small thickness. The dimension of the SU-8 micro-protrusion was 50 μm × 50 μm × 30 μm. The elastic moduli of PDMS, PI, gold, and SU-8 were 1.5 MPa, 2.5 GPa, 77.2 GPa, and 4.611 GPa, respectively. The Poisson's ratios of PDMS, PI, gold, and SU-8 were 0.48, 0.34, 0.44, and 0.252, respectively. A pressure of 68 kPa was applied to a rigid plate (2.5 mm by 2.5 mm) which was placed onto the P/T-unit.

Note S3: Thermal analysis of the sensing pixel.

A 3D FEM model was established in COMSOL to investigate the surface temperature of the sensing pixel. The transient model, from the bottom to the top layer, consisted of the PDMS substrate (thickness: 100 μm; thermal conductivity: 0.16 $W \cdot m^{-1} k^{-1}$; Heat capacity: 1460 J/ (kg· K); Density: 970 kg/m^3), the PI supporting layer (thickness: 2.5 μm; thermal conductivity: 0.3 $W \cdot m^{-1} k^{-1}$; Heat capacity: 1090 J/ (kg· K); Density: 1320 kg/m^3), the PI encapsulating layer (thickness: 2.5 μm; thermal conductivity: 0.3 $W \cdot m^{-1} k^{-1}$; Heat capacity: 1090 J/ (kg· K); Density: 1320 kg/m^3), and the SU-8 layer (thickness: 30 μm; thermal conductivity: 0.2 $W \cdot m^{-1} k^{-1}$; Heat capacity: 550 J/ (kg· K); Density: 3100 kg/m^3). The thickness of the Cr/Au layers (5/60 nm) was much smaller than that of the other layers such that it was reasonable to ignore them. The surface of sensing pixel maintained a constant temperature of 80 °C for 5 s.

Supplementary Figures

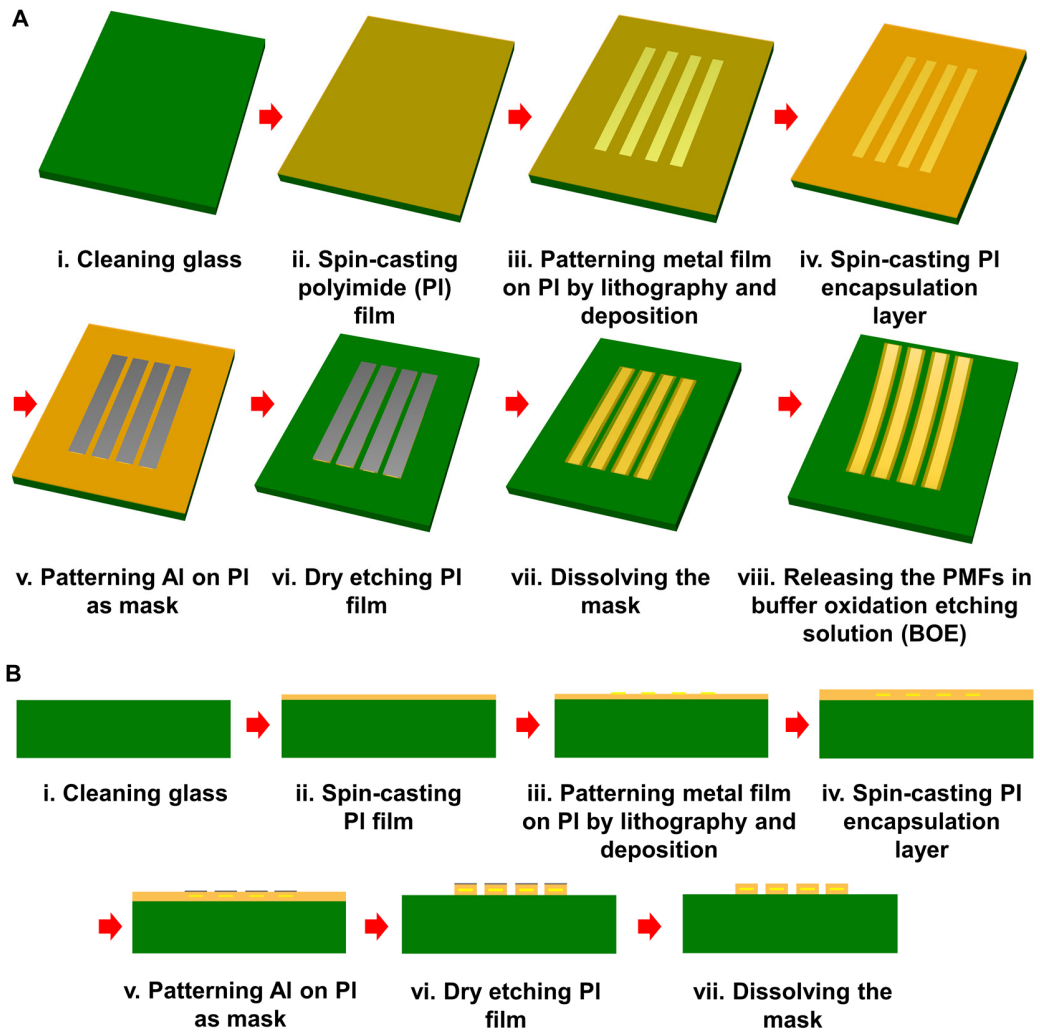

Fig. S1. Schematic illustrations of the fabrication process of the patterned metal films. (**A**) Perspective views of the fabrication process. (**B**) Cross-section views of the fabrication process.

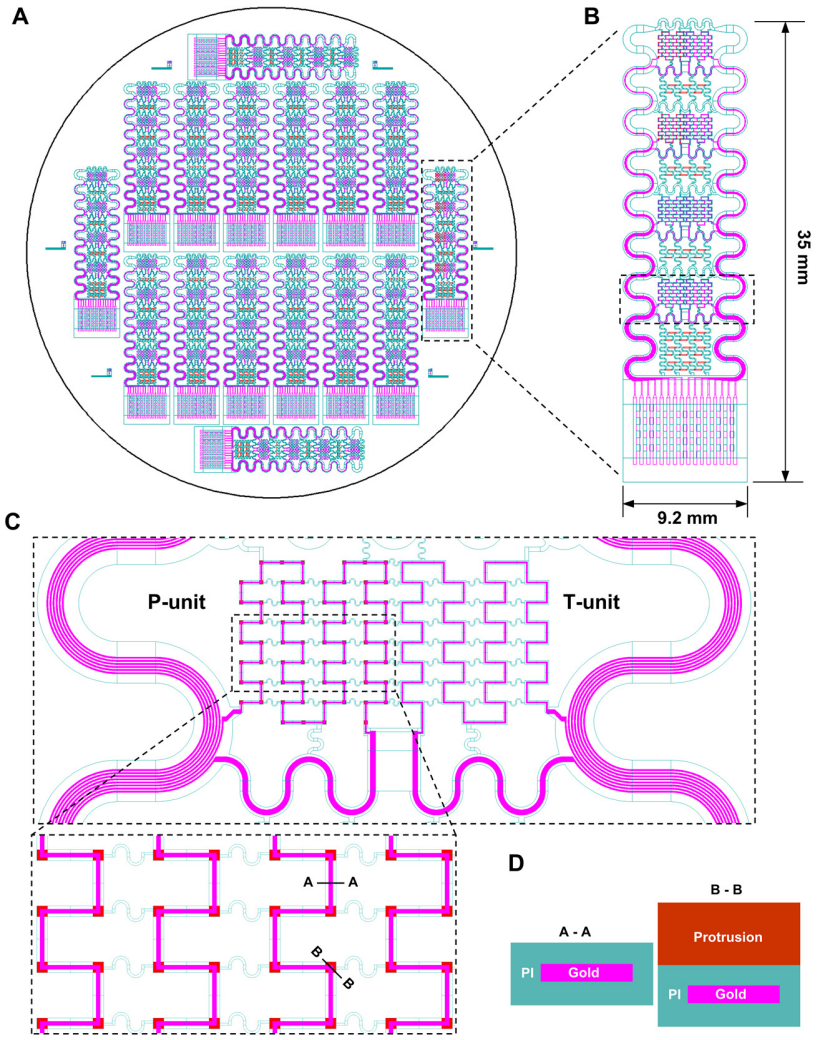

Fig. S2. Structural design of the 4-pixel e-skin prototype. (**A**) Design of the e-skins on a 4-inch glass. (**B**) Magnified view of a single e-skin. (**C**) Magnified views of a sensing pixel. (**D**) Cross-section views of the PMF of P-unit.

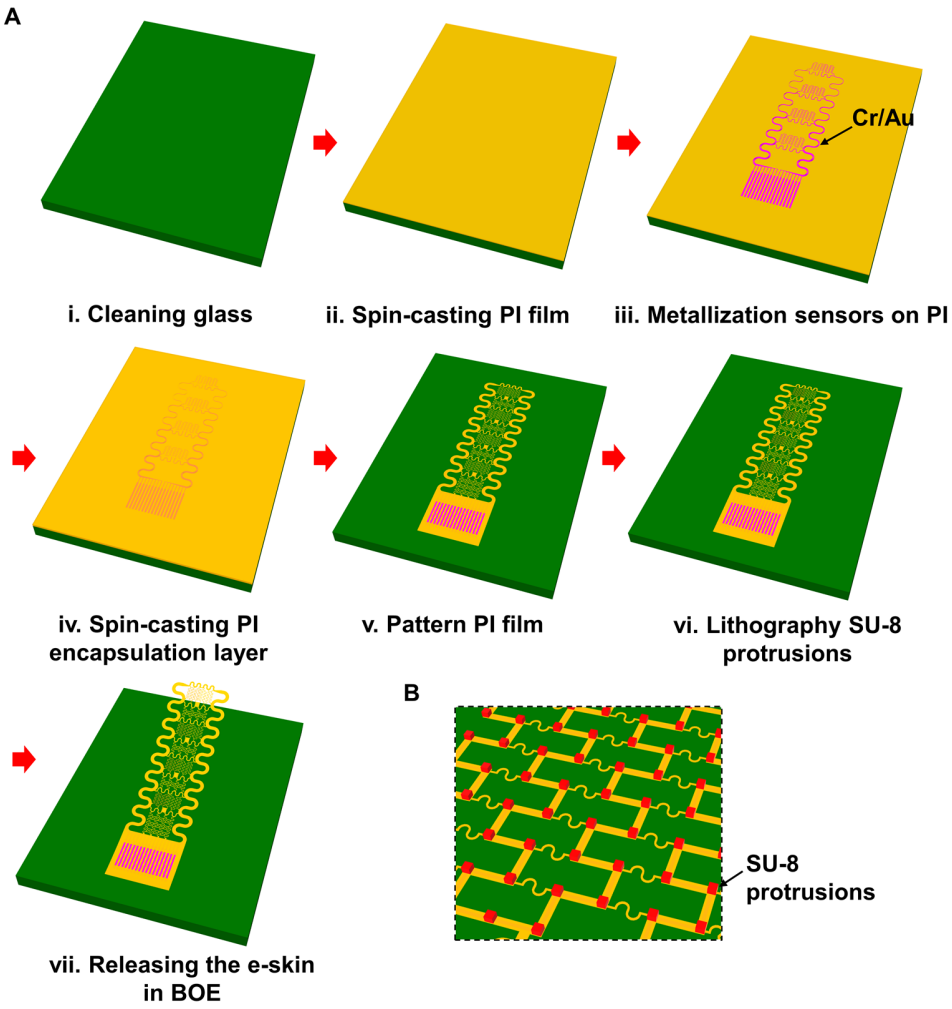

Fig. S3. Schematic fabrication process of the 4-pixel e-skin prototype. (**A**) Perspective views of the fabrication process. (**B**) Magnified view of the P-unit with SU-8 protrusions.

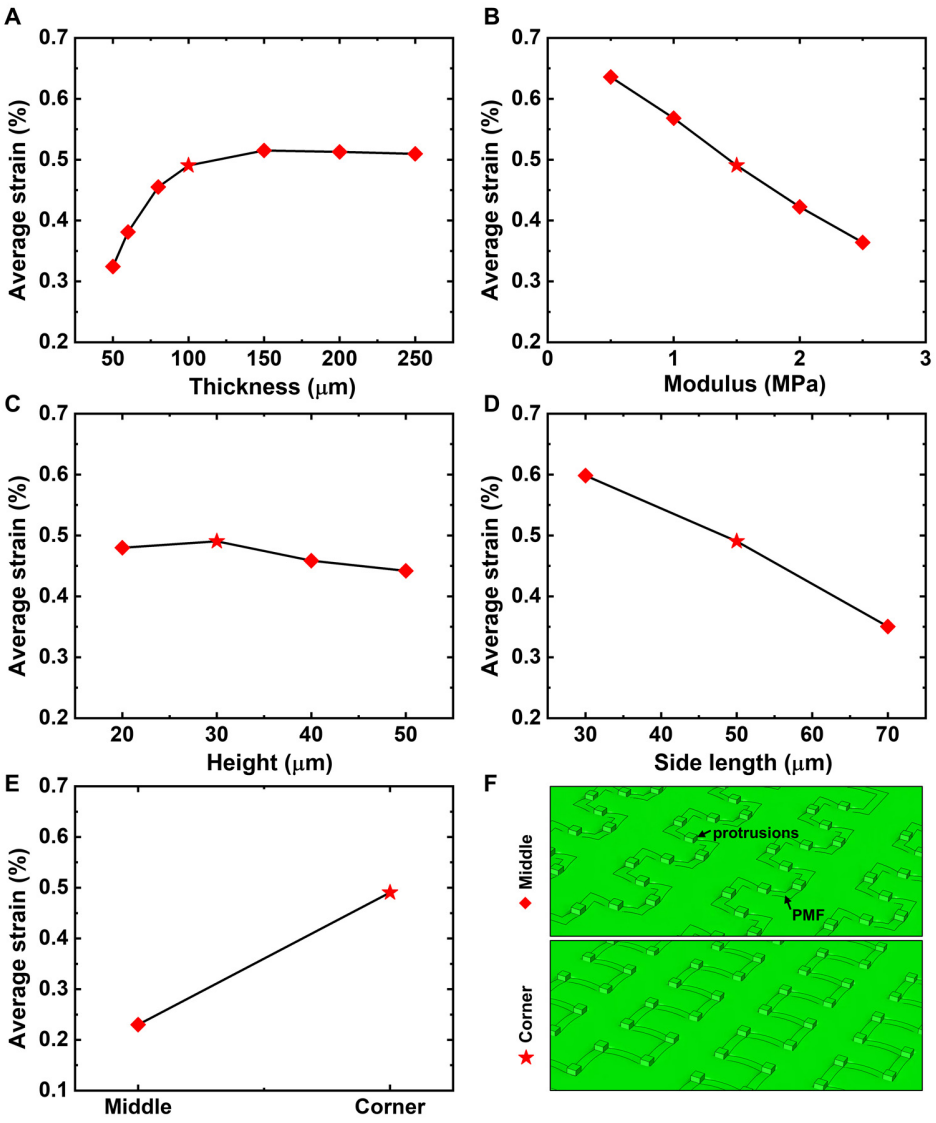

Fig. S4. Influences of the design parameters of the substrate and the protrusion on the average strain in the metal layer of the P-unit from FEA. The pentagrams denote the values of the fabricated devices in the paper. Influences of (**A**) the substrate thickness, (**B**) the substrate modulus, (**C**) the protrusion height, (**D**) the protrusion side length, and (**E**) the protrusion position on the average strain in the metal layer of the P-unit. (**F**) Images of the deformations of the P-unit corresponding to the different protrusion positions shown in (**E**).

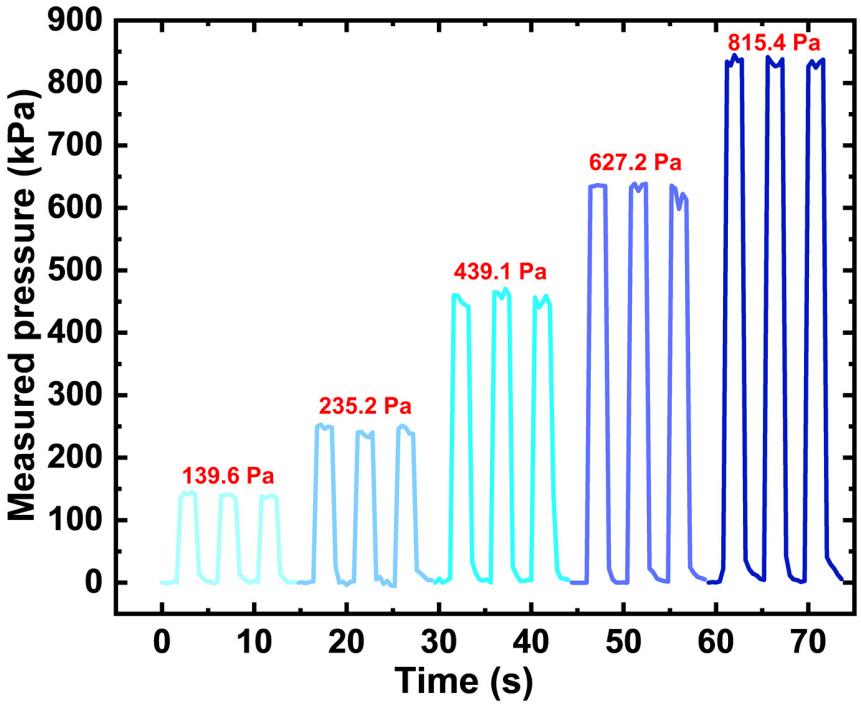

Fig. S5. The repeatability and accuracy of the P-unit towards five different levels of applied pressure. The red values represent the applied pressures.

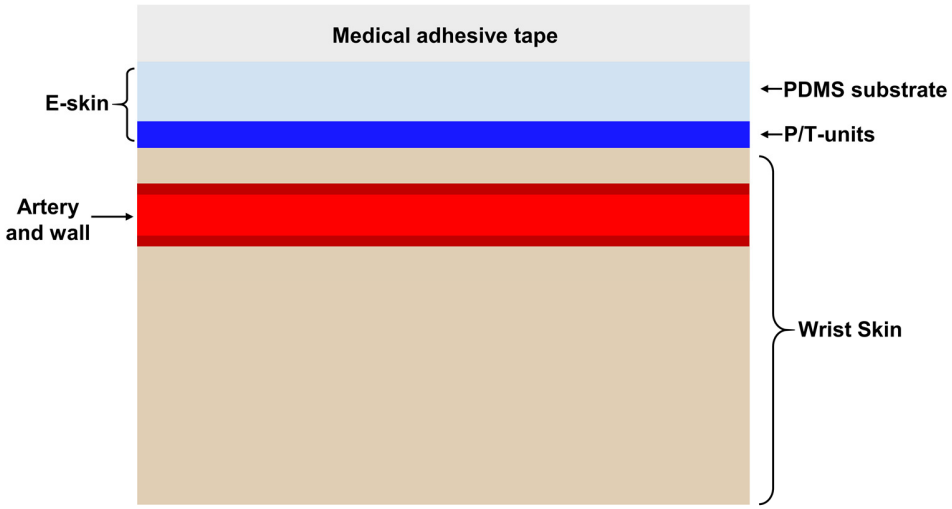

Fig. S6. Cross-section view of the measurement system of artery pulse.

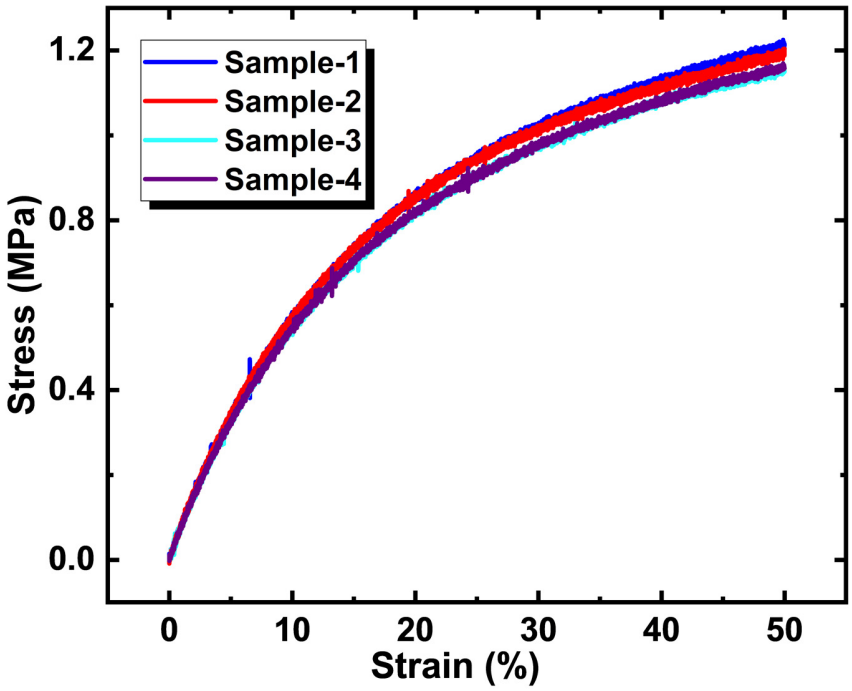

Fig. S7. Stress-strain curves of the stretchable medical adhesive tapes.

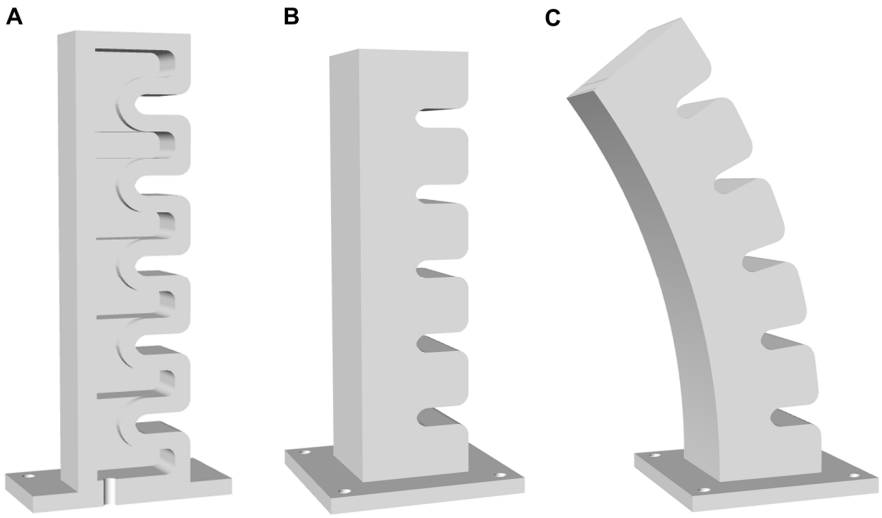

Fig. S8. Design of the flexible gripper. (**A**) Schematic of flexible finger, which is cut into halves to display inner structure. (**B**) The initial state of flexible finger. (**C**) The bending state of flexible finger.

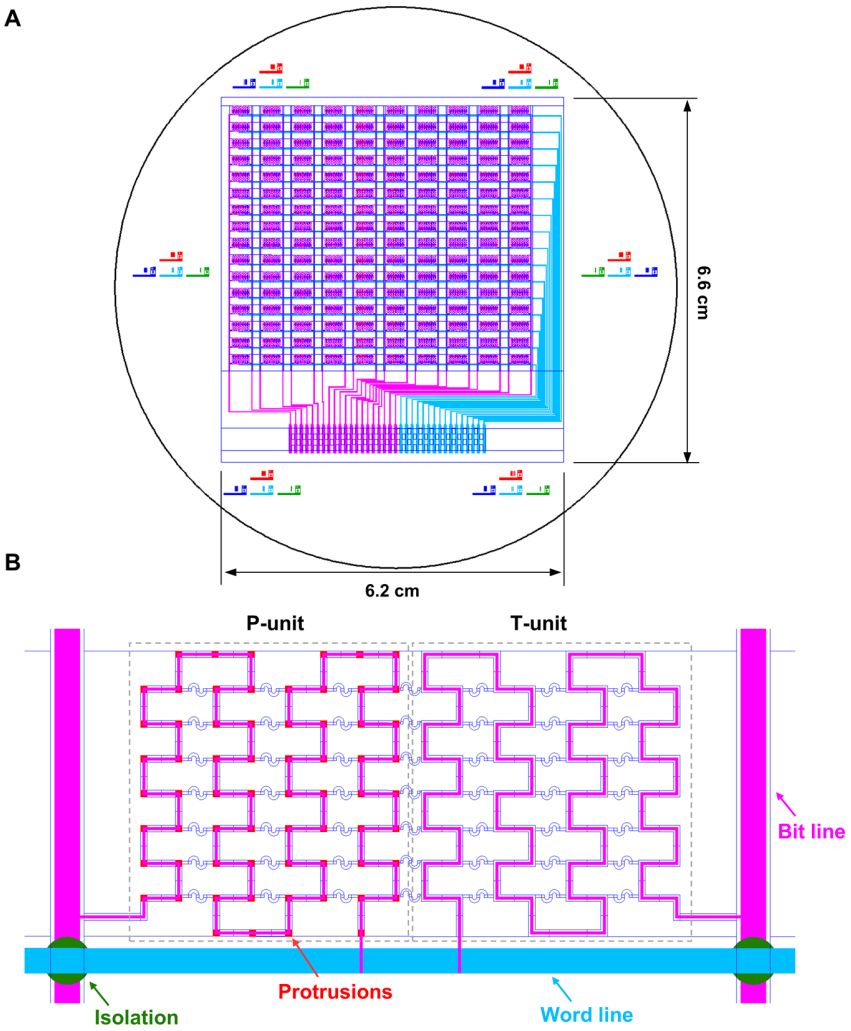

Fig. S9. Structural design of the flexible large-scale e-skin. (**A**) Design of the e-skins on a 4-inch glass. (**B**) Magnified views of a sensing pixel.

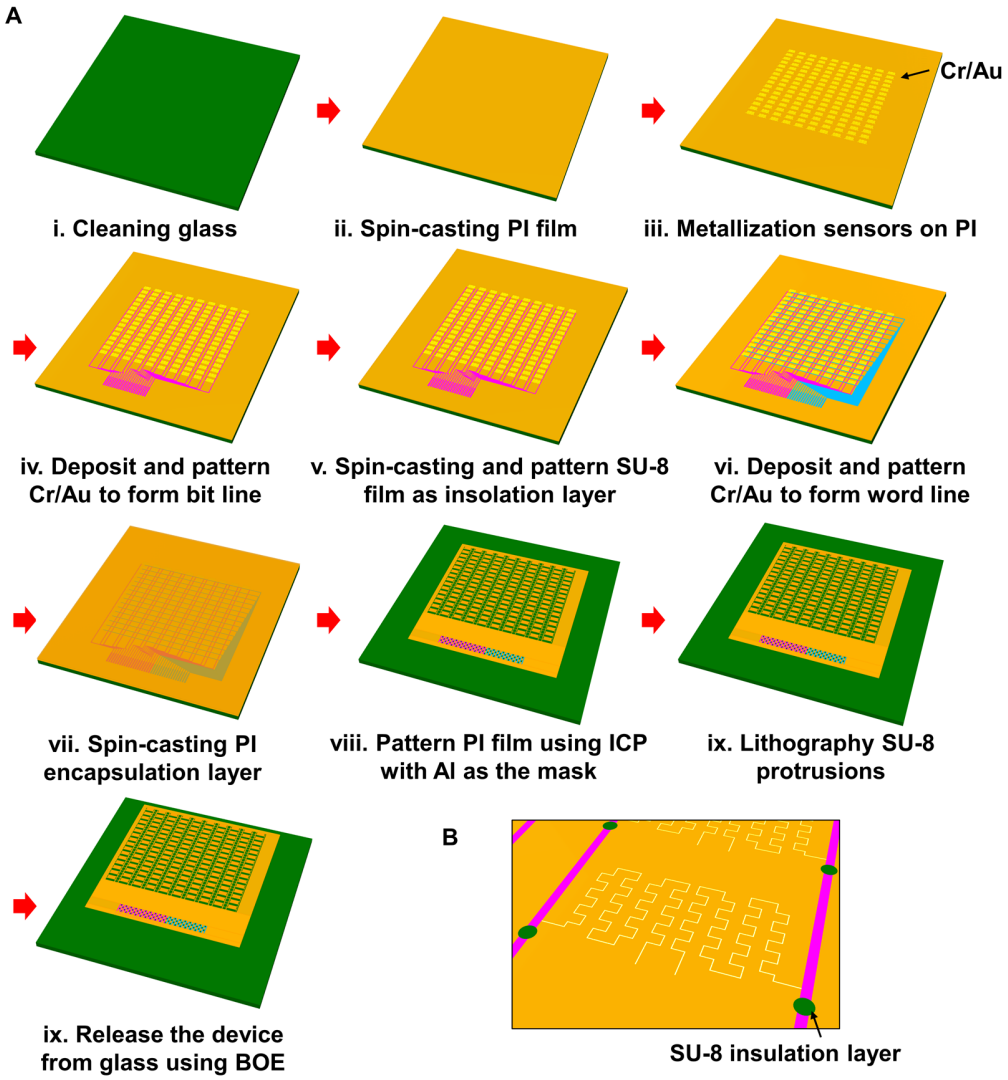

Fig. S10. Schematic fabrication process of the flexible large-scale e-skin. (**A**) Perspective views of the fabrication process. (**B**) Magnified view of the SU-8 insulation layer marked in (**A**)-v.

Supplementary Table

Table S1. Comparison of our device with other existing resistive temperature/pressure sensors with a broad linearity range of pressure detection.

Ref.	Type of pressure sensor	Linear range /kPa	Sensitivity of pressure /kPa^{-1}	Max. range /kPa	Response time /ms	Recovery time /ms	Type of temp. sensor	Sensitivity of temp. /K^{-1}	Max. range /K
This work	Resistive	80	2.02e-04	80	100	200	Resistive	8.3e-4	60
33	Resistive	0.5	15.1	60	40	40	-	-	-
34	Resistive	2.6	25.1	40	120	80	-	-	-
35	Resistive	0.5	0.88	4.5	500	1500	Resistive	8.2e-3	20
37	Resistive	2	0.26	10	-	-	-	-	-
38	Resistive	0.5	0.39	2.4	-	-	-	-	-
39	Resistive	1	9.7e-4	30	-	-	Resistive	-	-